Single-electron-detachment cross sections of Fe^-, Ru^-, Ni^-, Pd^-, and Pt^- in collisions with inert-gas atoms

Guangxin Min, Guannan Guo, Dedong Wang, and Xuemei Zhang*
Institute of Modern Physics, Fudan University, Shanghai 200433, People's Republic of China
and Applied Ion Beam Physics Laboratory, Fudan University, Key Laboratory of the Ministry of Education, Shanghai 200433, People's Republic of China
(Received 5 May 2017; published 19 June 2017)

The single-electron detachment (SED) cross sections of Fe^-, Ru^-, Ni^-, Pd^-, and Pt^- in collisions with inert-gas atoms are measured by using the growth-rate method. The projectile energy ranges from 10 to 30 keV. The cross sections increase as the impact velocity increases. For anions in the same element group, the data can be fitted into a straight line. The positions of fitting lines for different groups are different. In our velocity region, the intersections of fitting lines for different inert gases appear in the Cu group and the Ni group, but not in the Fe group. A model based on inelastic collision is used to explain the experimental results. Some conclusions are reached by analyzing the experimental data. The electron configuration of the anion plays an important role in SED cross sections. The mass relationship between the anion projectile and the inert-gas atom target is also an essential factor. The ionization energy of the target also has an influence on the SED cross sections.

DOI: 10.1103/PhysRevA.95.062706

I. INTRODUCTION

Anions, the combination of extra electrons and neutral atoms through the short-distance force, are widely distributed in our life. As an important branch of physics, the anion is a powerful tool to study atomic structure, atomic dynamics, and atomic collisions [1]. The single-electron detachment (SED) cross sections of the anions in collision with inert-gas atoms provide reliable experimental proof for theoretical calculation.

For decades, the SED experiment research has been focused on the low-energy and high-energy ranges. In the low-energy range, the anion velocity is much lower than the outermost electron orbital velocity of the anion. The collision process is often described by molecular or excimer models. In the high-energy range, the anion velocity is much higher than the outermost electron orbital velocity of the anion. The extra electrons of anion can usually be regarded as free, so the theory is commonly described by the Born approximation [2]. However, in the medium-velocity region, it is hard to set up a reasonable theoretical model.

In recent years, the SED cross sections of main-group-element anions have become more complete [3–11]. However, the data are still scarce for the transition elements. As is well known, transition elements have much more complex electronic structures, so it is difficult to describe the collision process between transition anions and atoms. The variation tendency of cross sections is usually described by an empirical formula.

In this paper the data of SED cross sections of Fe^-, Ru^-, Ni^-, Pd^-, and Pt^- colliding with inert-gas atoms when the projectile energy is ranging from 10 to 30 keV are obtained by the growth-rate method. In addition, the data are compared with previous experimental results. Qualitative explanations in different energy regions are also shown.

*zhangxm@fudan.edu.cn

II. EXPERIMENT

Figure 1 shows the main features of the experiment in a schematic way. Anions are produced by the cesium-sputter-type ion source. Anions are extracted by an electric field. An isotope separator is used to distinguish different ions and picks out the anions we need. The anions fly through a vacuum drift tube and then enter the collision chamber. The target-gas atoms are dispersed into the chamber. The density of the target gas is measured by an absolute pressure transducer. The beam is divided by the deflection plate after the collision section. After being separated by the electrostatic deflection plate, neutral particles and anions are detected by a multichannel-plate position-sensitive detector. The experimental setup has been described in Refs. [12–14]. Here we will just describe it briefly. The SED cross sections can be obtained by recording the counts of neutral particles and anions. The experimental method we use is the growth-rate method.

If the target-gas density is thin enough to meet the condition for a single collision, we can get the equations [15]

$$F_0 = \sigma_{-10}\pi + \tfrac{1}{2}[\sigma_{-11}\sigma_{10} - \sigma_{-10}(\sigma_{-10}+\sigma_{-11}+\sigma_{01}+\sigma_{0-1})]\pi^2, \tag{1}$$

$$F_0 = \frac{I_0}{I_{-1}+I_0+I_1}, \tag{2}$$

where $\pi = nl = C\frac{P}{kT}l = 7.26\times10^{16}\frac{Pl}{T}$; I_0 is the neutral particle beam intensity; I_{-1} is the anion beam intensity; I_1 is the positive ion intensity; σ_{-10} is the SED cross section; n (cm^{-3}) is the target-gas density; k is Boltzmann's constant; P (Pa) is the absolute pressure of the target gas; l (cm) is the length of the collision chamber; T (K) is thermodynamic temperature; and I_0, I_{-1}, and I_1 are measured simultaneously by a detector. In our experiment, we assume that the detector has the same detection efficiency for different charged particles and the measured beam intensities are seen as the produced beam intensities. By measuring I_0, I_{-1}, and I_1 at different gas pressures, we obtain F_0 with varying gas pressure. The cross

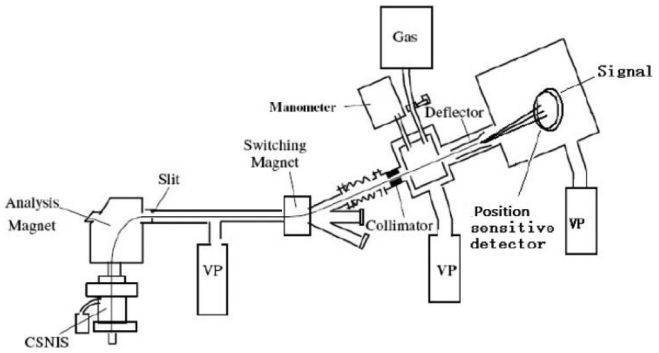

FIG. 1. Schematic diagram of the experimental device for measuring electron detachment cross sections of anions and atom collisions where CSNIS is caesium sputtering negative-ion source and VP is vacuum pump.

section can be obtained by curve fitting via Eqs. (1) and (2). The method has been used in our previous works [12,14] and is called the growth-rate method.

The main uncertainty in the experimental results comes from the following factors: (a) the uncertainty caused by the effective length of the chamber can be estimated as about ±2%, (b) the uncertainty caused by the statistical uncertainty of the particle count is estimated to be about ±3%, (c) the uncertainty caused by the pressure measurement is estimated to be about 0.25%, and (d) the uncertainty caused by the detection efficiency is estimated to be about 10.4%. The total experimental uncertainty is estimated to be 11.1%.

III. RESULTS AND DISCUSSION

The SED cross sections of Fe^-, Ru^-, Ni^-, Pd^-, and Pt^- in collisions with inert-gas atoms have been obtained; the experimental data are shown in Table I and Figs. 2–9. The results of Cu^-, Ag^-, and Au^- are from Refs. [13,14]. The SED cross sections in the energy ranging from 10 to 30 keV increase when the incident energy or incident velocity increases. The anions are divided into three element groups: The Fe group includes Fe^- and Ru^-; the Ni group includes Ni^-, Pd^-, and

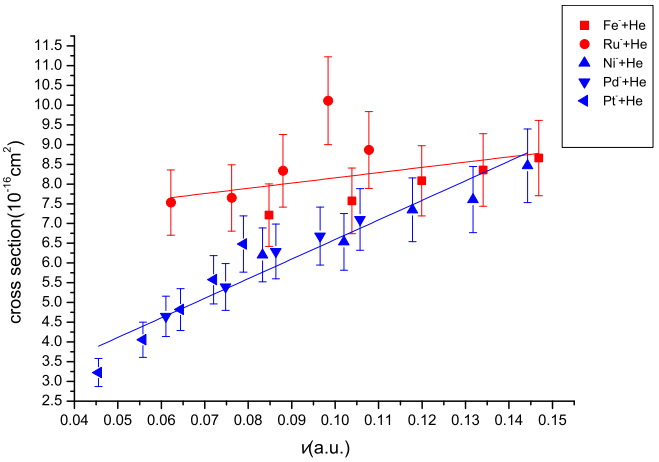

FIG. 2. The SED cross sections of Fe^-, Ru^-, Ni^-, Pd^-, and Pt^- in collisions with He.

TABLE I. The SED cross sections $\sigma(10^{-16}\,\mathrm{cm}^2)$ for Ni^-, Pd^-, Pt^-, Fe^-, Ru^-, Cu^-, Ag^-, and Au^- with inert-gas atoms and experimental errors $\Delta(10^{-16}\,\mathrm{cm}^2)$.

			Energy (keV)				
Element	Target	Parameter	10.0	15.0	20.0	25.0	30.0
$^{56}Fe^-$	He	σ	7.2	7.6	8.1	8.4	8.7
$^{56}Fe^-$	He	Δ	0.8	0.8	0.9	0.9	1.0
$^{56}Fe^-$	Ne	σ	9.6	8.9	9.7	11.4	11.1
$^{56}Fe^-$	Ne	Δ	1.1	1.0	1.1	1.3	1.2
$^{56}Fe^-$	Ar	σ	10.1	9.8	10.7	11.1	11.8
$^{56}Fe^-$	Ar	Δ	1.9	1.8	2.0	2.1	2.2
$^{56}Fe^-$	Kr	σ	7.8	9.0	10.5	12.3	10.3
$^{56}Fe^-$	Kr	Δ	0.9	1.0	1.2	1.4	1.1
$^{56}Fe^-$	Xe	σ	10.0	10.7	12.0	12.4	12.4
$^{56}Fe^-$	Xe	Δ	1.1	1.2	1.3	1.4	1.4
$^{104}Ru^-$	He	σ	7.5	7.6	8.3	10.1	8.9
$^{104}Ru^-$	He	Δ	0.8	0.8	0.9	1.1	1.0
$^{104}Ru^-$	Ne	σ	9.1	9.3	9.7	9.8	10.3
$^{104}Ru^-$	Ne	Δ	1.0	1.0	1.1	1.1	1.1
$^{104}Ru^-$	Ar	σ	9.0	9.6	9.9	10.1	10.0
$^{104}Ru^-$	Ar	Δ	1.0	1.1	1.1	1.1	1.1
$^{104}Ru^-$	Kr	σ	9.2	10.1	10.1	10.4	11.0
$^{104}Ru^-$	Kr	Δ	1.0	1.1	1.1	1.1	1.2
$^{104}Ru^-$	Xe	σ	10.2	11.8	11.8	12.0	12.4
$^{104}Ru^-$	Xe	Δ	1.1	1.3	1.3	1.3	1.4
$^{58}Ni^-$	He	σ	6.2	6.5	7.3	7.6	8.5
$^{58}Ni^-$	He	Δ	0.7	0.7	0.8	0.8	0.9
$^{58}Ni^-$	Ne	σ	4.7	4.8	4.9	6.0	6.1
$^{58}Ni^-$	Ne	Δ	0.5	0.5	0.5	0.7	0.7
$^{58}Ni^-$	Ar	σ	5.2	5.6	6.3	7.7	8.0
$^{58}Ni^-$	Ar	Δ	1.0	1.0	1.2	1.4	1.5
$^{58}Ni^-$	Kr	σ	5.8	7.2	7.6	8.6	8.6
$^{58}Ni^-$	Kr	Δ	0.6	0.8	0.8	0.9	0.9
$^{58}Ni^-$	Xe	σ	5.5	7.0	8.5	10.7	10.6
$^{58}Ni^-$	Xe	Δ	0.6	0.8	0.9	1.2	1.2
$^{108}Pd^-$	He	σ	4.6	5.4	6.3	6.7	7.1
$^{108}Pd^-$	He	Δ	0.5	0.6	0.7	0.7	0.8
$^{108}Pd^-$	Ne	σ	4.0	4.9	5.2	5.9	5.8
$^{108}Pd^-$	Ne	Δ	0.4	0.5	0.6	0.7	0.6
$^{108}Pd^-$	Ar	σ	3.7	4.4	4.8	5.7	6.4
$^{108}Pd^-$	Ar	Δ	0.4	0.5	0.5	0.6	0.7
$^{108}Pd^-$	Kr	σ	3.9	4.5	5.1	6.0	6.6
$^{108}Pd^-$	Kr	Δ	0.4	0.5	0.6	0.7	0.7
$^{108}Pd^-$	Xe	σ	3.6	4.6	5.0	6.2	7.9
$^{108}Pd^-$	Xe	Δ	0.4	0.5	0.5	0.7	0.9
$^{194}Pt^-$	He	σ	3.2	4.1	4.8	5.6	6.5
$^{194}Pt^-$	He	Δ	0.4	0.4	0.5	0.6	0.7
$^{194}Pt^-$	Ne	σ	3.7	4.3	4.7	5.3	6.1
$^{194}Pt^-$	Ne	Δ	0.4	0.5	0.5	0.6	0.7
$^{194}Pt^-$	Ar	σ	2.4	3.2	3.5	4.1	4.5
$^{194}Pt^-$	Ar	Δ	0.3	0.3	0.4	0.5	0.5

TABLE I. (*Continued*.)

Element	Target	Parameter	Energy (keV) 10.0	15.0	20.0	25.0	30.0
$^{194}Pt^-$	Kr	σ	1.9	2.5	3.3	3.8	4.4
$^{194}Pt^-$	Kr	Δ	0.2	0.3	0.4	0.4	0.5
$^{194}Pt^-$	Xe	σ	1.9	2.6	3.1	4.2	4.4
$^{194}Pt^-$	Xe	Δ	0.2	0.3	0.3	0.5	0.5
$^{63}Cu^-$	Ar	σ	2.8	3.2	6.0	6.6	5.6
$^{63}Cu^-$	Ar	Δ	0.5	0.6	1.1	1.2	1.0
$^{63}Cu^-$	Kr	σ	2.2	3.4	3.8	4.4	5.2
$^{63}Cu^-$	Kr	Δ	0.2	0.4	0.4	0.5	0.6
$^{63}Cu^-$	Xe	σ	3.7	4.4	6.4	6.5	7.7
$^{63}Cu^-$	Xe	Δ	0.4	0.5	0.7	0.7	0.9
$^{107}Ag^-$	Ar	σ	1.4	3.8	4.7	6.0	5.5
$^{107}Ag^-$	Ar	Δ	0.3	0.8	0.9	1.2	1.1
$^{107}Ag^-$	Kr	σ	2.0	2.4	2.5	3.0	3.1
$^{107}Ag^-$	Kr	Δ	0.2	0.3	0.3	0.3	0.3
$^{107}Ag^-$	Xe	σ	1.9	2.9	4.4	5.1	5.5
$^{107}Ag^-$	Xe	Δ	0.2	0.3	0.5	0.6	0.6
$^{197}Au^-$	Ar	σ	1.0	1.6	1.9	2.8	3.2
$^{197}Au^-$	Ar	Δ	0.2	0.3	0.4	0.6	0.6
$^{197}Au^-$	Kr	σ	1.3	1.7	2.4	2.6	2.8
$^{197}Au^-$	Kr	Δ	0.1	0.2	0.3	0.3	0.3
$^{197}Au^-$	Xe	σ	1.1	2.2	1.8	2.6	3.0
$^{197}Au^-$	Xe	Δ	0.1	0.2	0.2	0.3	0.3

Pt^-; and the Cu group includes Cu^-, Ag^-, and Au^-. For anions in the same group, the data can be fitted into a straight line. The positions of fitting lines for different groups are different. The fitting lines with different colors are shown in Figs. 2–9. From Figs. 2–6 the fitting lines of Fe^- and Ru^- are in the highest positions, the fitting lines of Cu^-, Ag^-, and Au^- are in the lowest positions, and the fitting lines of Ni^-, Pd^-, and Pt^- are in the middle positions. The cross sections of each group's

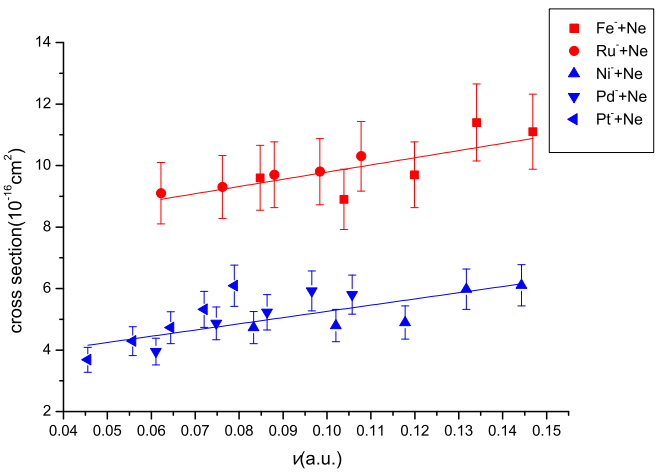

FIG. 3. The SED cross sections of Fe^-, Ru^-, Ni^-, Pd^-, and Pt^- in collisions with Ne.

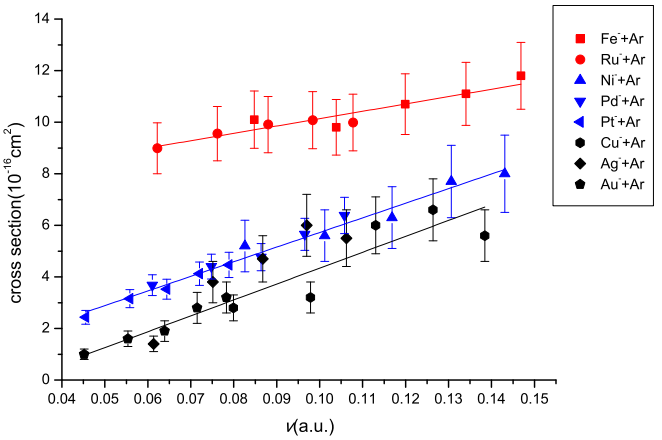

FIG. 4. The SED cross sections of Fe^-, Ru^-, Ni^-, Pd^-, Pt^-, Cu^-, Ag^-, and Au^- in collisions with Ar.

anions in collision with inert gases are shown in Figs. 7–9. For the Ni group and the Cu group, there are intersections of fitting lines, but there is no intersection for the Fe group.

In order to understand the experimental results better, we introduce an inelastic collision model. After the collision between the anion and the target atom, the kinetic energy of the incident anion should be divided into four parts: the residual kinetic energy of the incident ion, the kinetic energy of the target atom, the energy for target-atom ionization, and the energy for anion electron detachment. According to the theory of completely inelastic collisions in classical mechanics, the value of maximum energy ΔE_i can be transformed into the energies for the anion electron detachment and the target-atom ionization, which should be expressed by

$$\Delta E_{\mathrm{i}} = \frac{m_2}{m_1 + m_2} E, \tag{3}$$

where m_1 is the mass of the incident anion, m_2 is the mass of the target atom, and E is the incident kinetic energy of the anion. In the actual process, the collision is not the completely

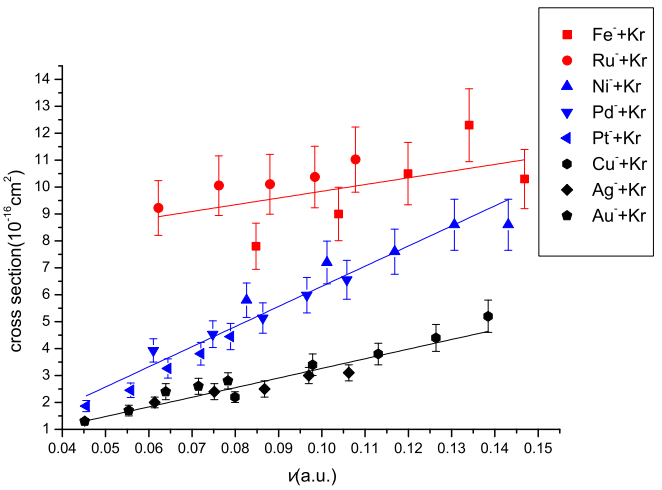

FIG. 5. The SED cross sections of Fe^-, Ru^-, Ni^-, Pd^-, Pt^-, Cu^-, Ag^-, and Au^- in collisions with Kr.

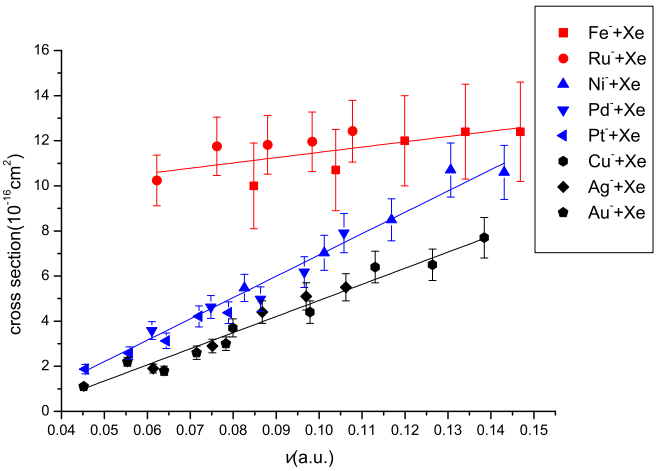

FIG. 6. The SED cross sections of Fe^-, Ru^-, Ni^-, Pd^-, Pt^-, Cu^-, Ag^-, and Au^- in collisions with Xe.

inelastic collision; a coefficient k should be introduced

$$\Delta E = k\Delta E_i = k\frac{m_2}{m_1 + m_2}E, \tag{4}$$

where ΔE is the total energy for the anion electron detachment and the target-atom ionization. As is well known, the single electron detachment process prefers a large-impact-parameter collision [16,17]. When a large-impact-parameter collision happens, the coefficient k is usually a small value. The fluctuation of the coefficient k can be ignored. Therefore, k is treated as a constant in (4) in the following analysis. Here ΔE provides the total energy for the ionization of the target atom and the detachment of the negative ion. For the same anion, the problem can be explained by two aspects. (a) If ΔE is large enough, ΔE will lead to both anion electron detachment and target-atom ionization. The lower the ionization energy of the target atom, the larger the remaining parts of the energy ΔE for the anion electron detachment, so the probability of electron detachment becomes larger. (b) If the ΔE is not big enough, only one type of electron-loss process could happen (anion electron detachment or target-atom ionization). If the target atom has lower ionization energy, the possibility of ionization of the target atom becomes larger. As a result, the probability of electron detachment of the anion becomes smaller.

Now, we explain the data.

Result 1. The cross sections increase with increasing incident velocity. From Eq. (4), for a certain incident anion, the bigger the incident velocity, the larger the E in the formula (4); ΔE becomes larger too. The bigger value of ΔE means that there is more energy used for the electron detachment of the anion. Therefore, the possibility of negative ion detachment becomes larger, which leads to the larger SED cross section.

Result 2. The electronic structures of different anions are listed in Table II from Ref. [18]. It is easy to understand that the electronic structures of anions from the same group are similar to each other; the trends of their cross sections are similar too. Comparing the electronic configurations of the negative ions from different groups in Table II, it could be found that the number of unpaired electrons of Fe^- and Ru^- is three and the number of unpaired electrons of Ni^-, Pd^-, and Pt^- is one.

TABLE II. Electronic structure of different anions [18].

Atom	Z	Atomic structure	Negative ion
Fe	26	$3d^6 4s^2$	$3d^7 4s^2$
Ru	44	$4d^7 5s$	$4d^7 5s^2$
Ni	28	$3d^8 4s^2$	$3d^9 4s^2$
Pd	46	$4d^{10}$	$4d^{10} 5s$
Pt	78	$5d^9 6s$	$5d^9 6s^2$
Cu	29	$3d^{10} 4s$	$3d^{10} 4s^2$
Ag	47	$4d^{10} 5s$	$4d^{10} 5s^2$
Au	79	$5d^{10} 6s$	$5d^{10} 6s^2$

The shells of Cu^-, Ag^-, and Au^- are full. A conclusion can be inferred that, the smaller the number of unpaired electrons, the more stable the anion. The steady state leads to the smaller probability for the electron detachment SED cross sections. The fitting lines of Fe^- and Ru^- are in the highest position and the fitting lines of Cu^-, Ag^-, and Au^- are in the lowest position. The fitting lines of Ni^-, Pd^-, and Pt^- are between them.

Result 3. Fitting lines intersect in Figs. 7 and 8, but no intersections appear in Fig. 9. The SED cross sections for Ni^-, Pd^-, and Pt^- in collisions with five kinds of inert gases are shown in Fig. 7. On the right-hand side of the intersections (higher-velocity region), the cross sections become bigger with the order of the target atoms from He to Xe increasing. On the left-hand side of the intersections (the lower-velocity part), however, the cross sections become smaller from He to Xe. In the lower-velocity region, the data are from Pt^-. If we put the masses of Pt^- and gas atoms into the formula (4), the values of $m_2/(m_1 + m_2)$ are as follows: 0.02 (He), 0.09 (Ne), 0.17 (Ar), 0.30 (Kr), and 0.40 (Xe). Putting them into the original formula (4), ΔE may be much smaller, which may only be enough for one type of ionization (anion electron detachment or target-atom ionization). Table III shows the ionization energies of inert gases. As we discussed above, if the target atom has smaller ionization energy, the possibility of ionization for the target atom will become larger. As a result,

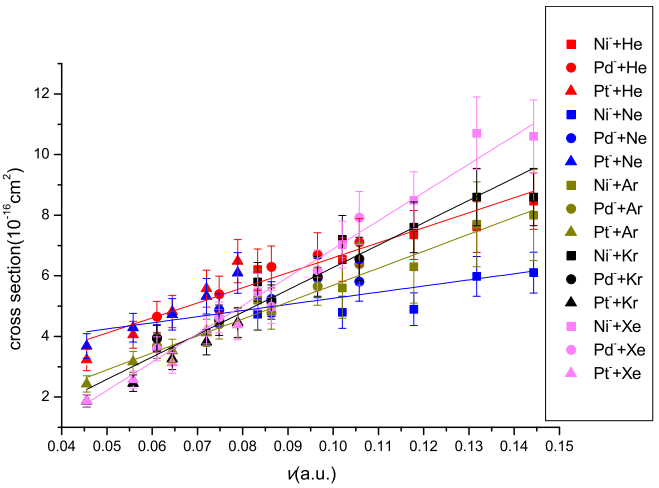

FIG. 7. The SED cross sections of Ni^-, Pd^-, and Pt^- in collisions with inert-gas atoms.

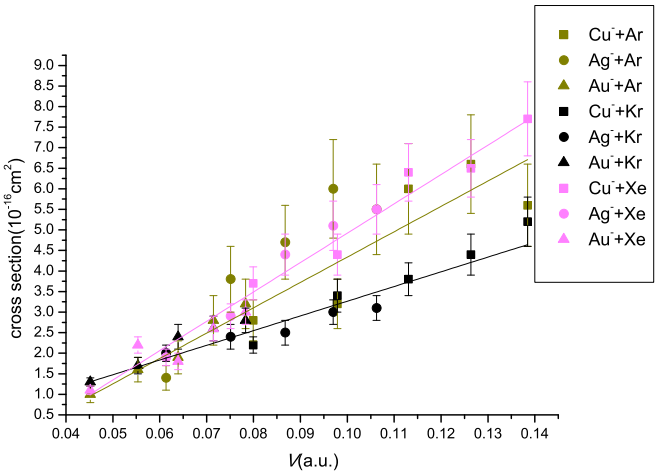

FIG. 8. The SED cross sections of Cu^-, Ag^-, and Au^- in collisions with inert-gas atoms.

the probability of anion electron detachment becomes smaller. As ionization energies decrease successively from He to Xe, the SED cross sections decrease. In the higher-velocity region, the data are from Ni^-. Putting the masses of Ni^- and gas atoms into the formula (4), the values of $m_2/(m_1+m_2)$ are as follows: 0.06 (He), 0.26 (Ne), 0.41 (Ar), 0.60 (Kr), and 0.70 (Xe). Much bigger values are obtained compared with those of Pt^-. Putting them into the original formula (4), ΔE will become larger than those impacted by Pt^-. Now ΔE may be big enough to cause both anion electron detachment and target-atom ionization. If the ionization energy of the target atom is large, the remaining energy for the anion electron detachment is relatively small. So the probability of anion electron detachment is small. As ionization energies decrease successively from He to Xe, the SED cross sections increase. Obviously, helium, which has a much smaller value (0.06), has small ΔE. This situation is similar to those impacted by Pt^-. Only one type of ionization (anion electron detachment or target-atom ionization) could happen. Due to the big ionization energy of He, the ionization of He become more difficult; it is much easier for the electron detachment of anion. This could

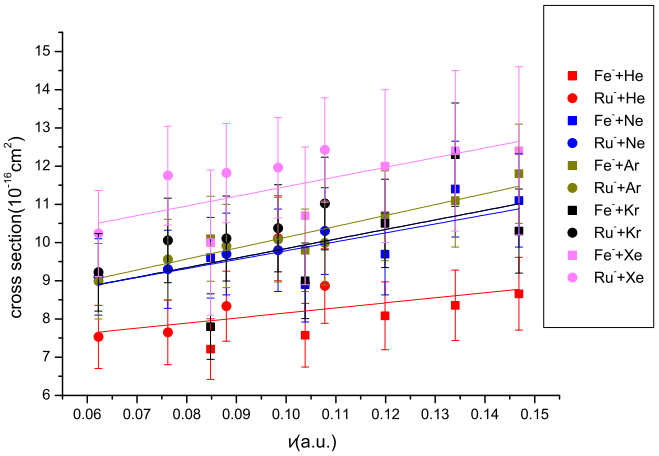

FIG. 9. The SED cross sections of Fe^- and Ru^- in collisions with inert-gas atoms.

TABLE III. Ionization energy of the inert-gas atom [19].

Atom	Mass	Ionization energy (eV)
He	4	24.6
Ne	20	21.36
Ar	40	15.8
Kr	84	14.0
Xe	131	12.1

be the reason why the cross sections of Ni^- in collisions with He are larger than expected in the higher-velocity part.

Now we use a similar analysis to explain Figs. 8 and 9. The SED cross sections for Cu^-, Ag^-, and Au^- in collisions with three kinds of inert gases are shown in Fig. 8. The fitting lines cross each other. On the right-hand side of the intersections, the cross sections of Xe are larger than those of Kr. However, the data of Ar are bigger than the result we expected, which is similar to the case of He in the Ni group. The data on the right-hand side of the intersections are contributed by Cu^-. The values of $m_2/(m_1+m_2)$ are as follows: 0.3883 (Ar), 0.5714 (Kr), and 0.6753 (Xe). Because of the fully occupied outermost shell, the anion states of the Cu group are more stable than those of the Ni group. The anions of the Cu group need more energy for electron detachment. So a larger ΔE is required for anion electron detachment and target-atom ionization. Maybe the value of $m_2/(m_1+m_2)$ (0.3883) for Ar is too small. Smaller ΔE may only be enough for one type of ionization (anion electron detachment or target-atom ionization). So the cross sections of Cu^- in collisions with Ar are larger than the result we expected. Figure 9 shows the SED cross sections for Fe^- and Ru^- in collisions with five kinds of inert gases. The obvious difference compared with the previous two groups is the absence of an intersection. According to the analysis of result 2, the states of the anions are unstable compared with the other two groups. The energy for anion electron detachment is much lower. Therefore, ΔE is big enough to lead to both anion electron detachment and target-atom ionization, though ΔE is much smaller in the lower-velocity region. In the whole velocity region, the same rule works. The cross sections of Ne, Ar, and Kr are very close to each other and it is hard to distinguish the positions of their fitting lines. Overall, as ionization energies decrease successively from He to Xe, the SED cross sections increase accordingly. The measurement is in good agreement with the inelastic collision model.

IV. CONCLUSION

The SED cross sections of Fe^-, Ru^-, Ni^-, Pd^-, and Pt^- in collisions with inert-gas atoms have been measured by the growth-rate method in the energy range from 10 to 30 keV. The main experimental uncertainty is below 11.1%. The cross sections all increase as the impact velocity increase. For the anions in the same element group, the data can be fitted into a straight line. The positions of fitting lines for different groups are different. In our velocity region, intersections of fitting lines for different inert gases appear in the Cu group and the Ni group, but no intersections appears in the Fe group. Based on the inelastic collision model, the main factors influencing

SED cross sections are as follows: (1) the velocity of incident anions, (2) the mass relationship between incident anions and target atoms, (3) the electronic structures of anions, and (4) the ionization energies of the target atoms.

ACKNOWLEDGMENTS

This work was supported by the Chinese National Science Foundation (Grant No. 11374062) and Shanghai Leading Academic Discipline Project No. B107.

[1] G. H. Gillespie and M. Inokuti, Phys. Rev. A **22**, 2430 (1980).
[2] M. Meron and B. M. Johnson, Phys. Rev. A **41**, 1365 (1990).
[3] J. S. Risley, in *Proceedings of the XIth International Conference on the Physics of Electronic and Atomic Collisions, Kyoto, 1979*, edited by N. Oda and K. Takayanagi (North-Holland, Amsterdam, 1980), pp. 619–630.
[4] R. W. L. McCullough and H. B. Gilbody, J. Phys. B **15**, 791 (1982).
[5] H. Tawara and A. Russek, Rev. Mod. Phys. **45**, 178 (1973).
[6] B. Hird, M. Bruyere, S. Fafard, and M. W. Orakzai, Can. J. Phys. **66**, 810 (1988).
[7] B. Hird and I. A. Abbas, Phys. Rev. A **31**, 3974 (1985).
[8] B. Hird and F. Rahman, J. Phys. B **16**, 3581 (1983).
[9] H. Luna, F. Zappa, M. H. P. Martins, S. D. Magalhães, G. Jalbert, L. F. S. Coelho, and N. V. de Castro Faria, Phys. Rev. A **63**, 052716 (2001).
[10] M.-Y. Song, M. Litsarev, V. Shevelko, H. Tawara, and J.-S. Yoon, Nucl. Instrum. Methods Phys. Res. Sect. B **267**, 2369 (2009).
[11] G. Jalbert, W. Wolff, S. D. Magalhães, and N. V. de Castro Faria, Phys. Rev. A **77**, 012722 (2008).
[12] J. Zhao, X. Bai, J. Li, X. Zhang, B. Wei, and Y. Zou, Nucl. Instrum. Methods Phys. Res. Sect. A **613**, 257 (2010).
[13] J. Ye, Z. Zhao, Y. Zhu, J. Li, and X. Zhang, At. Data Nucl. Data Tables **100**, 1189 (2014).
[14] J. Li, J. Zhao, X. Bai, B. Wei, and X. Zhang, J. Phys. B **44**, 025201 (2011).
[15] T. J. Kvale, J. S. Allen, A. Sen, X. D. Fang, and R. Matulioniene, Phys. Rev. A **51**, 1360 (1995).
[16] Z. Zhao, J. Li, and X. Zhang, Phys. Rev. A **88**, 042708 (2013).
[17] V. P. Shevelko, M. S. Litsarev, and H. Tawara, J. Phys. B **41**, 115204 (2008).
[18] T. Andersen, H. K. Haugen, and H. Hotop, J. Phys. Chem. Ref. Data **28**, 1511 (1999).
[19] F. Yang and J. H. Hamilton, *Modern Atomic and Nuclear Physics* (World Scientific, Singapore, 2010).